RAA 2019 Vol. **19** No. **1**, 15(8pp) doi: 10.1088/1674–4527/19/1/15

http://www.raa-journal.org *http://iopscience.iop.org/raa*

Research in Astronomy and Astrophysics

Climatological analysis of the seeing at Fuxian Solar Observatory

Li-Hui Chen[1], Zhong Liu[2,3] and Dong Chen[3]

[1] School of Resource Environment and Earth Science, Yunnan University, Kunming 650091, China; *chenlh@ynu.edu.cn*
[2] School of Astronomy and Space Science, University of Chinese Academy of Sciences, Beijing 100049, China
[3] Yunnan Astronomical Observatory, Chinese Academy of Sciences, Kunming 650011, China; *lz@ynao.ac.cn*

Received 2018 October 9; accepted 2018 November 7

Abstract There is a significant seasonal variation in the seeing of Fuxian Solar Observatory (FSO). The seeing in summer and autumn is better than that in winter and spring. The overall seeing is divided into the boundary layer seeing and free atmosphere seeing to investigate the climatic phenomena or meteorological events that might lead to seasonal variation in the seeing. The overall seeing was measured by the solar difference image motion monitor (SDIMM). The boundary layer seeing is calculated from the temperature difference between air and water. The analysis results show that the seasonal variation in seeing is caused by the alternation of subtropical high and westerly jet. The decrease of seeing in winter and spring at FSO is probably related to the westerly jet. A complete analysis of the seeing at FSO is given in this paper. It is also the first time to describe FSO's boundary layer seeing and its measurement method.

Key words: observational — high angular resolution — turbulence — site testing

1 INTRODUCTION

The location of Fuxian Solar Observatory (FSO) is $24°34'47''$ N and $102°57'02''$ E, at the northeast side of Fuxian Lake (Fig. 1), with an altitude of 1720 m above sea level. The New Vacuum Solar Telescope (NVST), with a 985 mm clear aperture, is the current primary observing facility at FSO (Liu et al. 2014). Due to the good seeing (Fried parameter) of FSO, a large number of high angular resolution data has been observed by NVST during the 24th solar cycle (Yang et al. 2015; Yan et al. 2015a,b; Ji et al. 2016). It is well known that seeing is a key parameter for researches based on high angular resolution (Shen et al. 2015; Xue et al. 2016; Liu et al. 2018), however the seeing at FSO is not perfect all year. It varies significantly with the seasons and is closely related to the regional climatic characteristics. In order to arrange observations and instruments of NVST more reasonably, it is necessary to know variation patterns of the seeing. Moreover, understanding the reasons for the variation in seeing is very important for future daytime astronomical site testing.

2 SEASONAL VARIATIONS IN THE SEEING OF FSO

The physical definition of seeing (Fried 1966) is the coherence diameter of the turbulent atmosphere in terms of Fried parameter r_0, in cm. Equation (1) (Goodman 1985) is a frequently used expression for measuring the Fried parameter. It is modified from the definition formula of the Fried parameter. In Equation (1), r_0 is the Fried parameter of the turbulent atmosphere in the zenith direction, λ is the wavelength of the observing band, γ is the zenith angle of the observed object, h is the height, $C_N^2(h)$ is the refractive index structure constant of the atmosphere and H is the total height of the turbulent atmosphere. In astronomical observations, seeing can also be expressed as the full width at half maximum (FWHM) of a star image resulting from a long exposure (an exposure time much longer than 1 second), in arcseconds. If not specified, seeing in this paper refers to the Fried parameter r_0 at the wavelength of 0.55 micron

$$r_0 = 0.185 \cos^{3/5}(\gamma) \left[\frac{\lambda^2}{\int_0^H C_N^2(h) dh} \right]^{3/5} . \quad (1)$$

The longterm site testing period of FSO was from 1999 to 2002 (Liu & Beckers 2001; Lou et al. 2001; Zhou 2002). During this period, seeing (in terms of Fried parameter r_0) was measured by the solar differential image motion monitor (SDIMM) that was first developed by the FSO team (Liu et al. 2000).

Figure 2 depicts the annual variation curve of the seeing at FSO. This curve shows significant seasonal variation

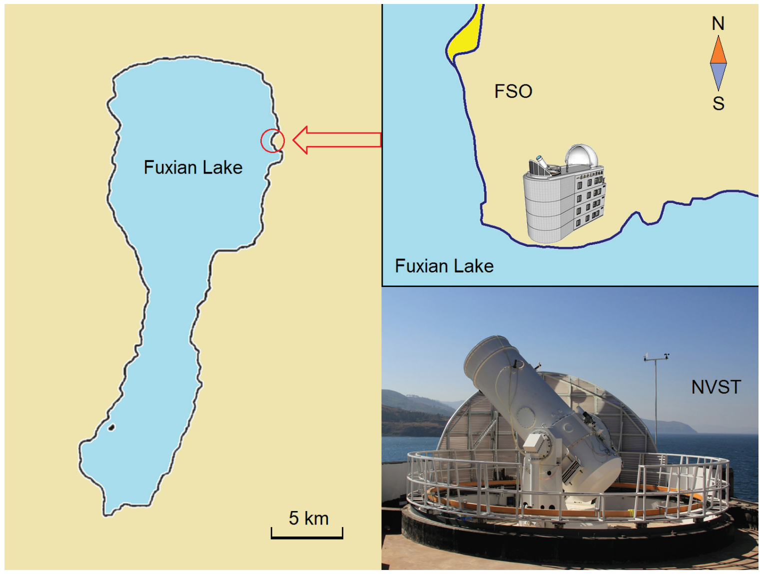

Fig. 1 The location of FSO and NVST.

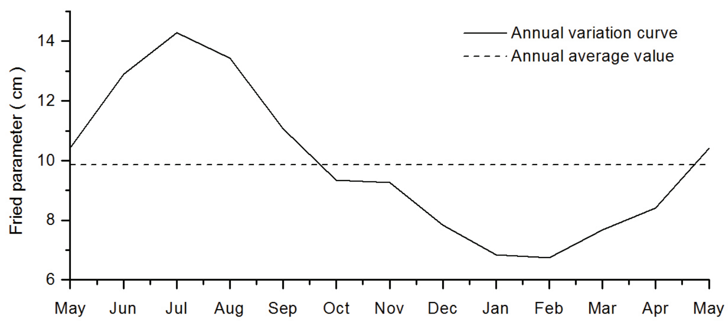

Fig. 2 Annual variation curve of the seeing at FSO. It is averaged from 2000 to 2002. All values were directly measured and not calibrated to zenith. The daily measurement usually lasts from 9 am to 4 pm Beijing time.

Table 1 Monthly, semiannual and annual average seeing* at FSO. All values in the table are in cm.

	May	Jun	Jul	Aug	Sep	Oct	Nov	Dec	Jan	Feb	Mar	Apr
Monthly	10.42	12.91	14.29	13.44	11.07	9.34	9.26	7.84	6.85	6.74	7.67	8.42
Semiannual	11.91						7.80					
Annual	9.85											

Notes: * All values are averaged from 2000 to 2002 and not calibrated to zenith.

in the seeing of FSO. The seeing is very good in summer and autumn, but in spring and winter, the seeing is lower than the annual average value. The first light of NVST was in September 2010. From then to now, the image quality of solar observations with NVST also clearly exhibited such a seasonal variation.

Table 1 lists some specific average seeing values at FSO during the period from September 1999 to December 2002. The annual average seeing was 9.85 cm. The average seeing in summer and autumn was 11.9 cm, while that in spring and winter was only 7.8 cm. In fact, the 7.8 cm daytime seeing is not bad for high angular resolution solar observation, which means that there is a high probability to operate the adaptive optics system successfully. Although the seeing is not bad in winter, considering that there are more clear days in winter than in summer at FSO (NIGLAS 1990), such an annual distribution of seeing is not very ideal.

Table 2 shows the sunshine duration of Kunming and Fuxian Lake. During the site survey of NVST in the 1990s,

Table 2 Monthly average sunshine duration* of Kunming and Fuxian Lake, in hours.

	May	Jun	Jul	Aug	Sep	Oct	Nov	Dec	Jan	Feb	Mar	Apr
Kunming	204	134	112	135	120	135	170	190	218	216	244	239
FSO	202	136	111	131	118	131	161	182	211	212	236	235

Notes: * All data are averaged from 1981 to 2010, provided by NMIC of China.

it was found that several candidate sites near Kunming, including the current site of FSO, have similar seasonal variations in seeing and sunshine duration. Considering that FSO is less than 50 km away from Kunming and has the same climate, it is easy to understand why these observation sites have the same seasonal variations. Finding out the underlying causes of this seeing distribution is very important for the ongoing solar site survey (Liu & Zhao 2013; Song et al. 2018) and the development of next generation large solar telescopes such as the Chinese Giant Solar Telescope (CGST) (Warner et al. 2018; Liu et al. 2012, 2016).

3 SEEING CALIBRATION AND SEPARATION

To investigate the seasonal variations in daytime seeing of an observation site, seasonal changes in the solar zenith angle should be considered. In addition, turbulence in the lower atmosphere is strongly dependent on ground heat conduction which may change with seasons. The change in dynamics of the higher atmosphere caused by regional or even global climate phenomena should also be considered. Seasonal variations in the seeing of FSO cannot be explained clearly by directly analyzing the observed data (Fig. 2 and Table 1) because all above aspects are mixed together in the data. In order to analyze the details separately, it is necessary to calibrate and further process the original data.

3.1 Calibrating Data to the Zenith

It is well known that the solar zenith angle changes with seasons. The latitude of FSO is 24.6° N, with the solar zenith angle being only 1° on the summer solstice and up to 48° on the winter solstice. Because the daytime seeing is measured by observing the Sun, the measured value of seeing (Fried parameter r_0) is proportional to $\cos^{3/5}(\gamma)$, where γ is the solar zenith angle (Eq. (1)). In order to represent the observation conditions more objectively, it is normally not necessary to calibrate the seeing with the zenith angle (Liu et al. 2014). But in the case of this paper, it is necessary to calibrate the seeing to the zenith in order to analyze seasonal seeing variations caused by climatic factors. The data could not be accurately calibrated with a large zenith angle (Goodman 1985). Only those data measured when the Sun is close to its daily highest altitude can be well calibrated. Therefore, the data selected for the zenith angle calibration were measured within an hour of noon time on each day.

Figure 3 shows two annual variation curves of the noon seeing at FSO. The first curve has not been calibrated to zenith while the other one has.

Comparing the two curves in Figure 3, we find that the standard deviation of the calibrated curve decreased from 2.7 to 2.3, and the relative standard deviation decreased from 25% to 20%. This shows that the seasonal change of solar zenith angle is one of the reasons for seasonal variation in the seeing. However, variation of the calibrated curve and its residual deviation clearly indicate that there must be other important climatic factors or meteorological events leading to seasonal variations in the seeing.

3.2 Separation of the Boundary Layer Seeing and Free Atmosphere Seeing

The Earth's atmosphere is usually divided into a boundary layer (Garratt 1994) and free atmosphere to investigate atmospheric turbulence and related phenomena. The boundary layer refers to the lower atmosphere, including the layer near the ground. The dynamics of the boundary layer are closely related to friction between air and the ground. Turbulence in the boundary layer largely depends on the local topography and temperature distribution of the ground. The boundary layer on the sea or a big lake is only a few hundred meters high (Garratt 1994) because the surface is fairly flat and there is little friction between air and water. The free atmosphere refers to the atmosphere above the boundary layer. It is not affected by friction with the ground. The dynamics of the free atmosphere are mainly determined by rotation of the Earth, the global temperature distribution and large-scale topography, rather than local geography factors. Because the formation and dynamics of the boundary layer and free atmosphere are different, it is necessary to divide the overall seeing into boundary layer seeing and free atmosphere seeing.

In the following discussion, r_0 represents the overall seeing of the whole atmosphere, r_{0B} is defined as the boundary layer seeing and r_{0F} is defined as the free atmosphere seeing. In Equation (1), integration of the refractive

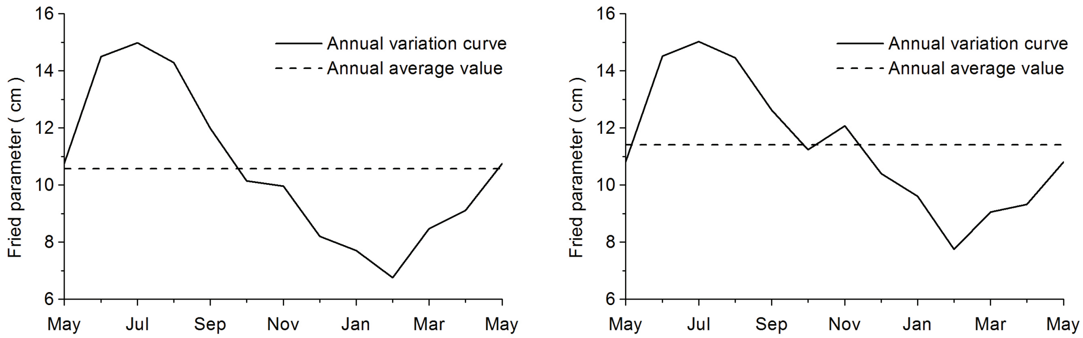

Fig. 3 Annual variation curves of the noon seeing at FSO. The left panel is the original curve. The right one has been calibrated to zenith. All data are averaged from 2000 to 2002.

index structure constant $C_N^2(h)$ can be expressed as

$$\int_0^H C_N^2(h)dh = \int_0^{H_B} C_N^2(h)dh + \int_{H_B}^H C_N^2(h)dh, \quad (2)$$

where H is the total height of the turbulent atmosphere and H_B is the height of the boundary layer. Another form of Equation (2) is easily derived by shifting Equation (1)

$$r_0^{-5/3} = r_{0F}^{-5/3} + r_{0B}^{-5/3} . \quad (3)$$

The overall seeing r_0 can be measured with a seeing monitor by observing the Sun (Liu et al. 2000). If r_{0B} can also be measured or calculated, then r_{0F} can be obtained from Equation (3). As mentioned above, Equation (1) is a frequently used expression for calculating seeing. To calculate r_{0B} by using Equation (1), it is necessary to know the refractive index structure constant $C_N^2(h)$ in the boundary layer. An expression for $C_N^2(h)$ was given by Fried as Equation (4) (Fried 1965)

$$C_N^2(h) = C_N^2(0)h^{-1/3} \exp\left(\frac{-h}{h_0}\right) . \quad (4)$$

In Equation (4), $C_N^2(0)$ is the refractive index structure constant of turbulent air near the ground, h is the height and h_0 is a constant equal to 3200. Equation (4) is suitable to calculate $C_N^2(h)$ in the boundary layer. Given $C_N^2(0)$, $C_N^2(h)$ can be calculated from Equation (4), and then r_{0B} can be further calculated by using Equation (1). The following paragraph describes how $C_N^2(0)$ was measured during the site testing period of FSO.

FSO is located on a small peninsula (Fig. 1) surrounded by lake water. The solar observation path is always across the lake from the morning to the afternoon. So, turbulence near the ground is mostly determined by heat conduction caused by the temperature difference ΔT between air and surface water. The refractive index structure constant of air near the ground $C_N^2(0)$ can be calculated from ΔT by the bulk aerodynamic method (bulk model) (Davidson et al. 1981; Andreas 1988; Frederickson et al. 1999). For the local environment and normal meteorological conditions at FSO, the specific relation between ΔT and $C_N^2(0)$ can be expressed by Equation (5) (Zhou 2002)

$$C_N^2(0) = (2.05\Delta T^2 + 2.37\Delta T + 1.58) \times 10^{-16} . \quad (5)$$

Here ΔT is equal to air temperature minus water temperature. In order to evaluate seeing near the ground at FSO, ΔT was measured from January 2001 to December 2002. The measurement was synchronized with the measurement of daytime seeing. Table 3 shows the monthly average ΔT and $C_N^2(0)$ at noon time at FSO.

Suppose the height of the boundary layer of Fuxian Lake is 500 m (Garratt 1994), and take the calibrated noon seeing as the overall seeing. By using the value of $C_N^2(0)$ in Table 3, r_{0B} and r_{0F} can be calculated from Equations (1), (3) and (4). The final results are displayed in Table 4.

3.3 Contributions of the Layered Atmosphere to the Overall Seeing

Table 4 indicates that the boundary layer seeing is much better than the free atmosphere seeing, but the relation between overall seeing and layered seeing is not a simple linear one. In order to investigate contributions of the layered atmosphere to the overall seeing, it is necessary to calculate the turbulence contribution rate of the boundary layer and the free atmosphere.

The items in Equation (2) have definite physical meanings. $\int_0^H C_N^2(h)dh$ represents the overall turbulence of the whole atmosphere, abbreviated as TH in this paper. $\int_0^{H_B} C_N^2(h)dh$ and $\int_{H_B}^H C_N^2(h)dh$ represent the turbulence of the boundary layer and the free atmosphere, abbreviated as TB and TF respectively. Then we have Equation (6)

$$\mathrm{TB/TH} + \mathrm{TF/TH} = \left(\frac{r_{0B}}{r_0}\right)^{-5/3} + \left(\frac{r_{0F}}{r_0}\right)^{-5/3} = 1 . \quad (6)$$

Table 3 Monthly Averaged ΔT* and $C_N^2(0)$ at FSO

		May	Jun	Jul	Aug	Sep	Oct	Nov	Dec	Jan	Feb	Mar	Apr
ΔT	(°C)	2.89	2.06	1.40	0.95	0.49	–0.26	–1.30	–1.85	–1.30	1.89	3.41	3.54
$C_N^2(0)$	$(10^{-16} \cdot \mathrm{m}^{-2/3})$	25.5	15.2	8.9	5.7	3.2	1.1	2.0	4.2	2.0	13.4	33.5	35.6

Notes: *ΔT is a signed parameter equal to air temperature minus water temperature in this paper.

Table 4 The overall seeing*, the boundary layer seeing and free atmosphere seeing, in cm, at FSO.

	May	Jun	Jul	Aug	Sep	Oct	Nov	Dec	Jan	Feb	Mar	Apr
r_0	10.82	14.52	15.03	14.46	12.63	11.25	12.07	10.40	9.62	7.76	9.05	9.32
r_{0F}	13.70	18.25	17.16	15.60	13.06	11.35	12.30	10.73	9.74	8.25	11.39	12.13
r_{0B}	21.18	28.94	39.71	52.03	73.16	139.09	98.56	62.27	98.14	31.21	18.00	17.33

Notes: * The overall r_0 is the noon seeing which has been calibrated to the zenith (the right panel in Fig. 3).

The ratio TB/TH can be defined as the turbulence contribution rate of the boundary layer, and TF/TH can be defined as the turbulence contribution rate of the free atmosphere. Table 5 shows the specific turbulence contribution rates of the layered atmosphere in different months.

As can be seen from Table 5, the annual turbulence contribution rate of the boundary layer is only 16%, while that of the free atmosphere is up to 84%. Compared with the boundary layer, the free atmosphere contributes more to the overall turbulence. Table 4 also shows that the overall seeing of FSO greatly depends on the free atmosphere seeing. In other words, the boundary layer seeing is so good that it does not have a significant impact on seasonal variation in the overall seeing of FSO.

According to Equation (2), the correlation between overall seeing and free atmosphere seeing can be expressed by the linear correlation coefficient between $r_0^{-5/3}$ and $r_{0F}^{-5/3}$. In fact, this correlation coefficient is as high as 0.89 at FSO. Considering the high turbulence contribution rate of the free atmosphere, it is clear that the seasonal variation in overall seeing originates from the variation in free atmosphere seeing.

4 CLIMATOLOGICAL ANALYSIS OF THE SEEING AT FSO

Since the seeing of the boundary layer and the seeing of the free atmosphere have been separated from the overall seeing, variations in seeing of the boundary layer and the free atmosphere can be analyzed separately to investigate the corresponding climatological reasons.

4.1 Boundary Layer

Figure 4 shows the boundary layer seeing and the temperature difference between air and water at FSO. The boundary layer seeing is very good. It is not the cause of the seasonal variation in the overall seeing, but excellent boundary layer seeing is a necessary condition for excellent overall seeing at FSO.

Excellent boundary layer seeing is due to the small temperature difference between air and surface water. In general, the smaller the temperature difference is, the better the boundary layer seeing becomes. This can be explained by the local climate. The water temperature is higher than the air temperature in winter. The temperature rises rapidly with the increase of solar radiation in spring. Since the heat capacity of water is larger than that of air and land, the rise of water temperature is slower than that of air temperature. If this trend continues, the temperature difference between air and water will keep increasing in summer and lead to poor boundary layer seeing. However, the subtropical high begins to control Fuxian Lake in May. Humid monsoons from the Indian Ocean and the Pacific Ocean enter this region alternately (NIGLAS 1990). Cloudy weather reduces solar radiation on the ground and slows the rise in air temperature. The temperature difference between air and water begins to decrease. After autumn, the water temperature gradually rises above the air temperature. As a result of the above regional climate characteristics, the temperature difference between air and water in Fuxian Lake is very small (Table 3). This is the reason why FSO has very good boundary layer seeing throughout a year, especially from August to the following January.

4.2 Free Atmosphere

Figure 5 displays a comparison between free atmosphere seeing and overall seeing at FSO. Both curves show similar seasonal variation patterns. As discussed in Section 3, variation in free atmosphere seeing is the primary source of overall seeing.

Analyzing seasonal variations in the free atmosphere seeing requires regional and even global climate data of the upper atmosphere. The climate data in this paper are from the National Meteorological Information Center (NMIC)

Table 5 Turbulence contribution rates of the boundary layer and the free atmosphere at FSO.

	May	Jun	Jul	Aug	Sep	Oct	Nov	Dec	Jan	Feb	Mar	Apr	Annual
TB/TH	0.33	0.32	0.20	0.12	0.05	0.02	0.03	0.05	0.02	0.10	0.32	0.36	0.16
TF/TH	0.67	0.68	0.80	0.88	0.95	0.98	0.97	0.95	0.98	0.90	0.68	0.64	0.84

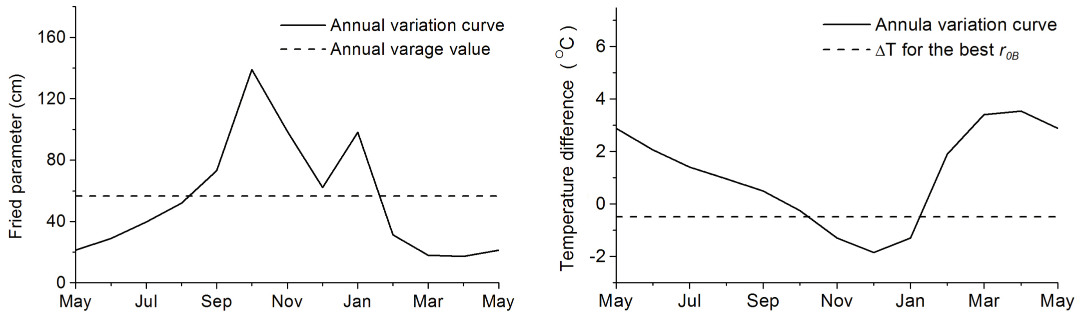

Fig. 4 Annual variation curves of the boundary layer seeing (*left panel*) and the temperature difference between air and surface water (*right panel*) at FSO. The data are from Tables 3 and 4.

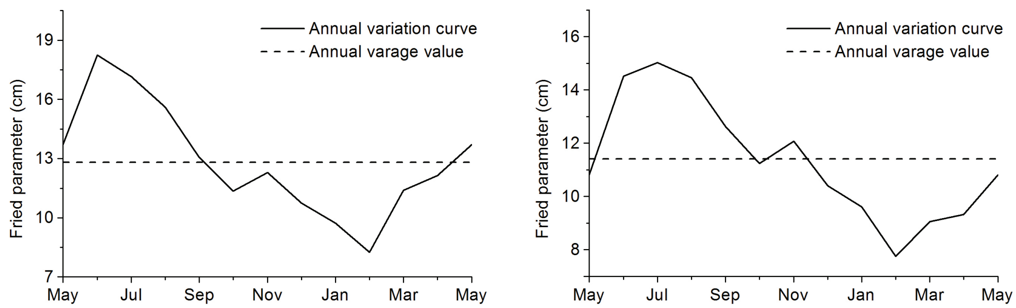

Fig. 5 Annual variation curves of the free atmosphere seeing (*left panel*) and the overall seeing (*right panel*) at FSO. The data are from Table 4.

of China. Climate data on the upper atmosphere were measured by sounding balloons released at Kunming from 1981 to 2010, including the data on temperature, wind speed and geopotential height of the upper atmosphere. The distance between the balloon launch point and FSO is less than 60 km, which does not affect the validity of upper atmospheric climate data.

Figure 6 depicts the distribution of temperature and wind velocity with height in the troposphere. As shown in the left panel of Figure 6, the border between the troposphere and stratosphere is at an altitude of 18 000 m where there is an obvious temperature inversion layer. This famous inversion layer has a certain contribution to the free atmosphere seeing (Hufnagel & Stanley 1964; Goodman 1985), but does not vary seasonally. There is neither obvious seasonal temperature variation between this border and the altitude of 3000 m, nor is there any stable seasonal temperature inversion layer. In contrast, seasonal variation in wind speed of the troposphere is apparent. As shown in the right panel of Figure 6, at an altitude of around 12 500 m, the average wind speed in winter and spring is four times higher than that in summer and autumn. Such a significant seasonal variation in wind speed of the troposphere is induced from seasonal alternations of the subtropical high and the westerly jet. In central Yunnan, including Fuxian Lake, the subtropical high dominates the monsoon season from May to October. The dry season from November to April is dominated by the westerly jet. The center of the westerly zone even moves southward to 26° N in spring, while its range of influence extends to 20° N (Schiemann et al. 2009).

Figure 7 shows annual wind speed variation curves at different altitudes. Wind speed at a geopotential height of 200 hPa (around a height of 12 400 m) is important for the analysis of seasonal variations in seeing. This height is identified as the position of the axis of the westerly jet by related researches on climatology (Schiemann et al. 2009). The linear correlations between wind speed and seeing of

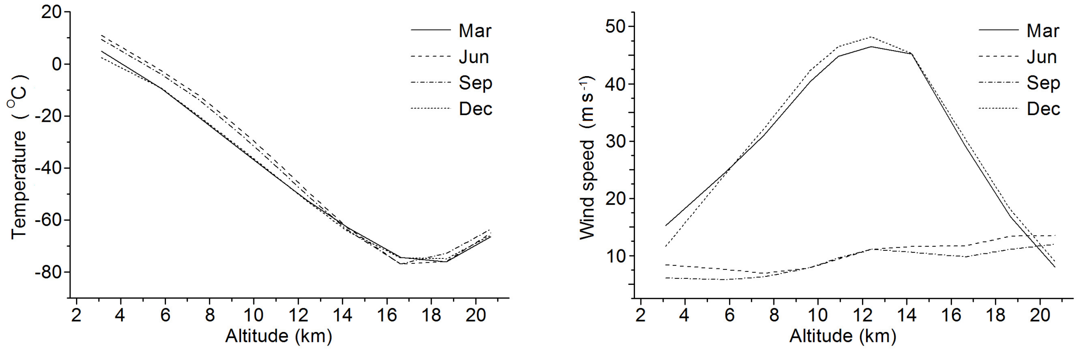

Fig. 6 The left panel shows temperature curves with height in different months. The right panel displays wind speed curves with height in different months. The data are from NMIC of China.

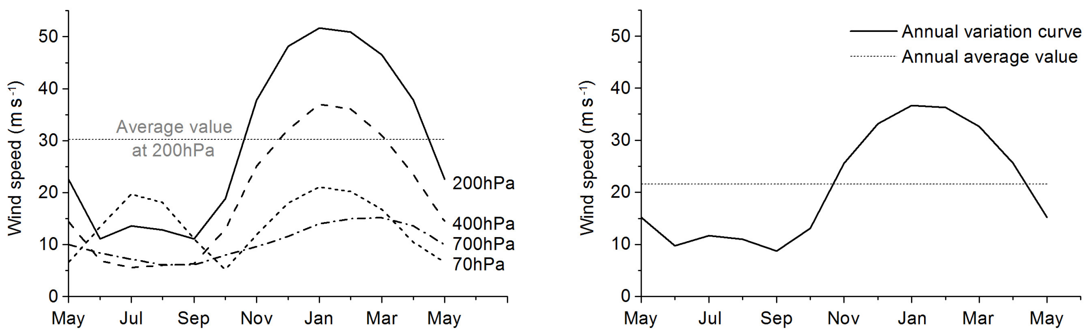

Fig. 7 The left panel shows annual wind speed variation curves at different altitudes. The right panel is the annual wind speed curve averaged from 700 hPa to 70 hPa. The geopotential height of 700 hPa corresponds roughly to an altitude of 3120 m in this case, 400 hPa corresponds roughly to 7540 m, 200 hPa corresponds roughly to 12 400 m and 70 hPa corresponds roughly to 18 700 m. The data are from NMIC of China.

Table 6 Linear correlation coefficients between wind speed and seeing of the free atmosphere (r_{0F}).

Geopotential height	700 hPa	500 hPa	400 hPa	300 hPa	200 hPa	100 hPa	70 hPa
Correlation coefficient	–0.70	–0.83	–0.85	–0.84	–0.82	–0.64	–0.12

the free atmosphere are calculated (Table 6). For layers with geopotential heights from 500 hPa to 200 hPa, correlation coefficients are more, in absolute value, than -0.8. This means that there is a strong negative correlation between the seasonal variation in wind speed and the seasonal variation in seeing. The greater the wind speed is, the worse the seeing becomes. Reynolds number of the air at a geopotential height of 200 hPa is calculated by taking the Fried parameter as the characteristic size. In the season dominated by the westerly jet, Reynolds number is on the order of 10^4. It is suitable for the development of small scale turbulence. In the monsoon season dominated by the subtropical high, Reynolds number is very close to the order of 10^3. The small-scale turbulence tends to dissipate and the atmosphere is more stable. It should be noted that the above analysis is fairly preliminary.

The results shown in Table 6 do not mean that there must be a linear relation between wind speed and seeing. The mechanism of this phenomenon is not simple and is beyond the scope of this paper.

5 CONCLUSIONS

The overall seeing of FSO varies significantly with seasons. It is mainly contributed by the free atmosphere and is closely related to seasonal change in the climate. In the monsoon season (from May to Oct) dominated by the subtropical high, the atmosphere is stable and the overall seeing is very good. In the dry season (from Nov to the following Apr) dominated by the westerly jet, the upper atmosphere moves fast and the overall seeing is lower than the annual average. There is a strong correlation between variation in seeing of the free atmosphere and variation in wind speed of the upper atmosphere. This indicates that the decrease of seeing in the dry season at FSO is probably related to the westerly jet. The mechanism of this phenomenon is still an open issue.

Finally, it should be noted that this work, especially the results shown in Table 4 and Table 5, is very helpful for the development and operation of adaptive optics and multi-conjugate adaptive optics (Rao et al. 2016, 2018) systems associated with NVST.

Acknowledgements The authors appreciate Professor Ruwei Lu for his excellent plan for measuring the air temperature and water temperature at FSO. The authors are also grateful for Professor Jie Cao for his recommendation on key climate researches. This work was supported by the National Natural Science Foundation of China (U1831210), Yunnan University first-class discipline construction fund (C176210215) and the talents program of Yunnan province. All the climate data are provided by the National Meteorological Information Center of China. Dr. Yuchao Chen and Dr. Yuliang Fang assisted the authors in processing some of the data. Dr. Yunfang Cai and Dr. Yongyuan Xiang aided the authors with text editing. The authors would like to express great appreciation to all the people who have participated in the site testing of FSO. Without their hard work, there would not be seeing data stemming from this effort.

References

Andreas, E. L. 1988, Journal of the Optical Society of America A, 5, 481

Davidson, K. L., Schacher, G. E., Fairall, C. W., & Goroch, A. K. 1981, Appl. Opt., 20, 2919

Frederickson, P. A., Davidson, K. L., Zeisse, C. R., & Bendall, C. S. 1999, in Proc. SPIE, 3763, Propagation and Imaging through the Atmosphere III, ed. M. C. Roggemann & L. R. Bissonnette, 230

Fried, D. L. 1965, Journal of the Optical Society of America (1917–1983), 55, 1427

Fried, D. L. 1966, Journal of the Optical Society of America (1917–1983), 56, 1372

Garratt, J. R. 1994, Earth Science Reviews, 37, 89

Goodman, J. W. 1985, Statistical Optics (New York: John Wiley and Sons)

Hufnagel, R. E., & Stanley, N. R. 1964, Journal of the Optical Society of America (1917–1983), 54, 52

Ji, K.-F., Xiong, J.-P., Xiang, Y.-Y., et al. 2016, RAA (Research in Astronomy and Astrophysics), 16, 78

Liu, Y., & Zhao, L. 2013, MNRAS, 434, 1674

Liu, Y., Xiang, Y., Erdélyi, R., et al. 2018, ApJ, 856, 17

Liu, Z., & Beckers, J. M. 2001, Sol. Phys., 198, 197

Liu, Z., Deng, Y., Jin, Z., & Ji, H. 2012, in Proc. SPIE, 8444, Ground-based and Airborne Telescopes IV, 844405

Liu, Z., Ji, H., Jin, Z., Lin, J., & Deng, Y. 2016, in Society of Photo-Optical Instrumentation Engineers (SPIE) Conference Series, 10012, Integrated Modeling of Complex Optomechanical Systems II, 1001204

Liu, Z., Lou, K., Zhang, R. L., Ru-Wei, L. U., & Beckers, J. 2000, Publications of the Yunnan Observatoty, 4, 018

Liu, Z., Xu, J., Gu, B.-Z., et al. 2014, RAA (Research in Astronomy and Astrophysics), 14, 705

Lou, K., Liu, Z., Zhang, R., Lu, R., & Wu, M. 2001, Progress in Astronomy, 19, 147

NIGLAS, C. 1990, Fuxian Lake, eds., S. C, Sun (Beijing: China Ocean Press), in Chinese

Rao, C.-H., Zhu, L., Rao, X.-J., et al. 2016, RAA (Research in Astronomy and Astrophysics), 16, 23

Rao, C., Zhang, L., Kong, L., et al. 2018, Science China Physics, Mechanics, and Astronomy, 61, 89621

Schiemann, R., Lüthi, D., & Schär, C. 2009, Journal of Climate, 22, 2940

Shen, Y., Liu, Y., Liu, Y. D., et al. 2015, ApJ, 814, L17

Song, T. F., Wen, Y. M., Liu, Y., et al. 2018, Sol. Phys., 293, 37

Warner, M., Rimmele, T. R., Pillet, V. M., et al. 2018, in Society of Photo-Optical Instrumentation Engineers (SPIE) Conference Series, 10700, 107000V

Xue, Z., Yan, X., Cheng, X., et al. 2016, Nature Communications, 7, 11837

Yan, X. L., Xue, Z. K., Pan, G. M., et al. 2015a, ApJS, 219, 17

Yan, X.-L., Xue, Z.-K., Xiang, Y.-Y., & Yang, L.-H. 2015b, RAA (Research in Astronomy and Astrophysics), 15, 1725

Yang, S., Zhang, J., & Xiang, Y. 2015, ApJ, 798, L11

Zhou, D. 2002, Characteristics of the Near-ground Atmospheric Turbulence, Master's Thesis, Graduate University of CAS, Yunnan Astronomical Observatory